COMMUNICATION

Side-Chain Molecular Engineering of Triazole-Based Donor−Acceptor Polymeric Photocatalysts with Strong Electron Push−Pull Interactions

Zhipeng Luo,[a] Xiaowen Chen,[a] Yuanyuan Hu,[a] Xiong Chen,[a]* Wei Lin,[a] Xiaofeng Wu,[b] Xinchen Wang[a]*

[a] Z. Luo, X. Chen, Y. Hu, Prof. X. Chen, Prof. W. Lin, Prof. X. Wang
State Key Laboratory of Photocatalysis on Energy and Environment, College of Chemistry
Fuzhou University
Fuzhou 350116 (P. R. China)
E-mail: chenxiong987@fzu.edu.cn; xcwang@fzu.edu.cn
[b] Dr. X. Wu
Materials Innovation Factory, Department of Chemistry
University of Liverpool
Liverpool L69 7ZD (UK)

Abstract: By the integration of electron-deficient alkyl chain anchored triazole (TA) moieties and electron-rich pyrene units into the polymer skeleton, a new series of donor-acceptor (D-A) type semiconductive polymers were generated, bearing satisfactory light-harvesting ability and suitable bandgaps. Benefiting from the minimized exciton binding energy along with strongest D-A interaction and favorable hydrophilicity, P-TAME exhibits an outstanding photocatalytic H_2 evolution rate of ~100 μmol h^{-1} (10 mg polymer, $AQY_{420\ nm}$ = 8.9%) and H_2O_2 production rate of ~190 μmol h^{-1} (20 mg polymer) under visible light irradiation, superior to most currently reported polymers. Besides, all these polymers can mediate water oxidation reactions to evolving O_2. Thus, these TA-based polymers open a new avenue for tailor-made efficient photocatalysts with broad photocatalytic activities.

The key issue in photocatalysis is the exploitation of efficient and stable photocatalysts to enable high-performance for solar-to-chemical energy conversion, which is still a long-term task. Owing to the unique properties such as versatile synthetic methods, broad light-harvesting ranges, and tunable electronic structures[1], polymer photocatalysts have garnered intensive research interest as a new family of semiconductor photocatalysts. To date, various polymer photocatalysts have been investigated, e.g., polymeric carbon nitride[2], covalent organic frameworks[3], linear polymers[4], and conjugated microporous polymers[5], etc.

Due to the low dielectric constant characteristics, charge separation and transport could be largely impeded during photocatalysis with polymeric substances, thereby affecting photocatalytic performance. Constructing donor-acceptor (D-A) polymer systems have been clarified as a reliable protocol to facilitate charge separation and migration[2b-c, 4b, 5b, 6]. However, very limited electron-acceptor motifs have been explored up to date, with dibenzothiophene-*S*,*S*-dioxide (FSO) and benzothiadiazole (BT)-based compounds be the most focus (Scheme 1a)[7]. To this end, developing a novel type of electron-acceptors to enrich the variety of D-A type polymer photocatalysts with fabulous photocatalytic activity is desired.

1*H*-1,2,4-triazole (TA) and its derivatives feature attractive electron-transport and hole-blocking properties, originating from their highly electron-deficient nature (Scheme 1b). Besides, the TA scaffold could be modified readily to showcase different characteristics. Indeed, they have been widely used to construct functional materials for diverse purposes, e.g., organic light-emitting diodes[8], polymer electrolyte membrane fuel cells[9], organic optical waveguides[10], organic photovoltaic cells[11], and others[12]. Accordingly, we envisage TA moiety could be an appealing acceptor candidate to build a set of novel D-A-type polymer photocatalysts, which have not been explored. Meanwhile, the N-rich atomic structure for TA units may act as the active sites during photocatalysis[13], contributing to the analysis and understanding of the reaction mechanism. Moreover, by engineering the TA skeleton, such properties, including photon absorptions, energy level structures, charge dissociation and transport, and the interface interactions with water, might be varied, ultimately leading to controllable photocatalytic functions.

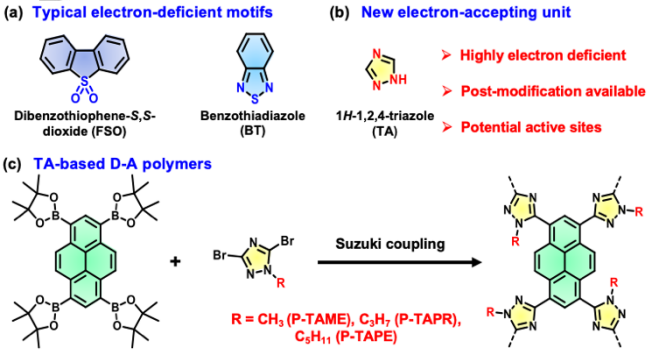

Scheme 1. a) Typical electron-deficient motifs. b) New electron-accepting unit used in this study. c)The synthetic routes for the TA-based D-A type polymer photocatalysts.

In this context, herein, a proof-of-concept study on the TA-based D-A conjugated polymers (P-TA-CPs, Scheme 1c) with structural embedded molecular engineering level electron push-pull interaction was conducted along with the investigation of the influence of side chain engineering on charge generation and migration kinetics. Firstly, electron-rich pyrene (Py) building blocks and electron-deficient TA moieties were integrated into the polymer skeletons, generating built-in electric fields and strong electron push-pull interactions to promote charge separation and transfer. When side alkyl chains with different lengths were incorporated into the TA units, the bandgaps and their alignments, hydrophilicity, and D-A interactions were further varied,

elucidating by both experimental and theoretical studies. These findings would provide crucial information for the design and modulation of side chains for promoting charge separation and migration kinetics in these D-A conjugated polymer photocatalysts, achieving efficient photocatalytic performance.

To synthesize the targeted polymers, a typical Suzuki-Miyaura polycondensation reaction was conducted (Scheme 1c, for details see the Supporting Information). All the polymers obtained were insoluble in common organic solvents and water, featuring amorphous nature as revealed by their broad powder X-ray diffraction (PXRD) signals (Figure S1). As displayed in the FT-IR spectra (Figure S2), the signals at ~1450-1750 cm^{-1}, ~1270-1300 cm^{-1}, and ~1440 cm^{-1} attributed to aromatic C=C as well as C-N and C=N in the TA moieties, respectively[1b, 14, 15]. The structural information of the polymers was further unraveled by the solid-state ^{13}C NMR spectra (Figure 1a). The signals at 0-50 ppm could be ascribed to different alkyl chains of the polymers. The peaks in the range of ~116-139 ppm originated from the carbons of Py units. The signals shown at ~153 and ~161 ppm belonged to C atoms in the TA ring.

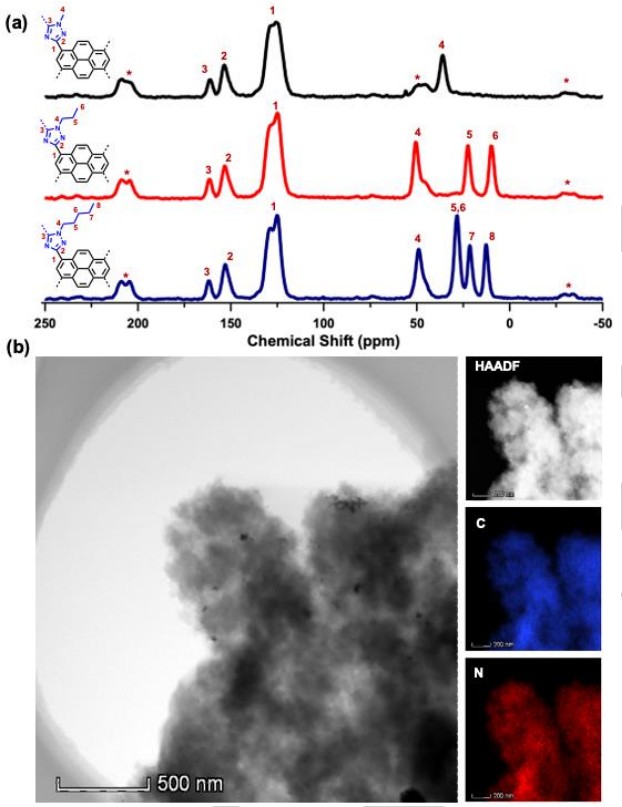

Figure 1. a) Solid-state ^{13}C NMR spectra of P-TA-CPs. b) TEM image of P-TAME with elemental maps for C and N.

X-ray photoelectron spectroscopy (XPS) was applied to investigate the chemical composition and structural features of these polymers. These polymers were mainly composed of C and N with a small amount of O, presumably stemmed from the atmospheric water or O_2 adsorption on the surface (Figure S3a). The C 1s XPS spectra of these polymers could be deconvoluted into two major peaks located at ~284.8 and 286.3 eV, attributed to the aromatic C=C species and the C=N bonds in the TA units, respectively (Figure S3b)[16]. Moreover, the N 1s XPS spectra of these polymers could be divided into two major peaks, assigned to the N atoms of C-N (~399.0 eV) and C=N (~401.0 eV) in the TA species (Figure S3c)[16c, 17]. The elemental analysis data (Table S1) indicated that the elemental compositions of P-TA-CPs were close to their theoretical values. All these results evidenced the successful preparation of desired P-TA-CPs.

An aggregated shape of all these polymers verified by scanning electron micrograph (SEM) images (Figure S4-S6). The morphology of the polymers can be further uncovered by transmission electron microscopy (TEM) images (Figures 1b and S7-S8). Besides, the high-angle annular dark field scanning transmission electron microscopy (HAADF STEM) elemental mapping images revealed the C and N elements were homogeneously distributed inside the polymers. The porosity of these polymers was assessed by N_2 sorption isotherm tests, affording the specific Brunauer−Emmett−Teller surface areas in a range of 675-19 $m^2\ g^{-1}$ (Figure S9). The P-TAME with the shortest alkyl chain exhibited the best porosity, which is conducive to mass transfer and enhanced photocatalytic activity.

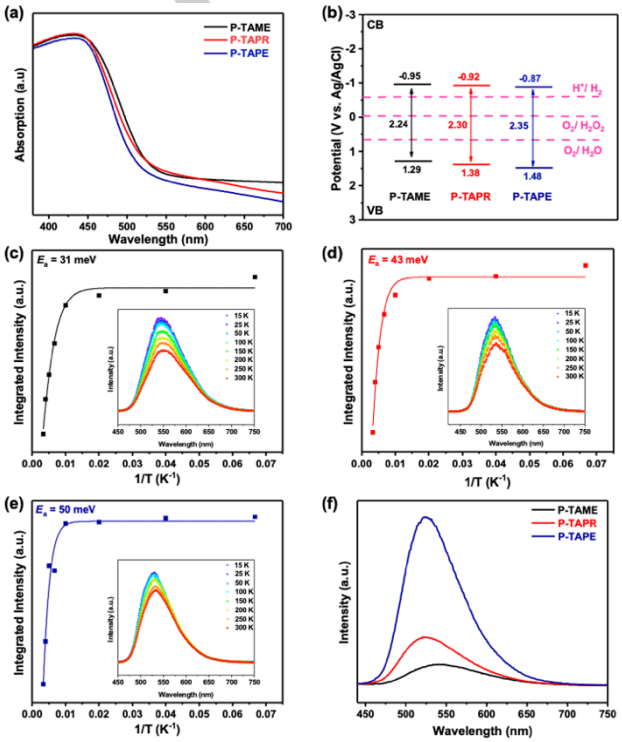

Figure 2. a) UV-vis DRS, and b) band alignments of P-TA-CPs. Integrated PL emission intensity as a function of temperature from 15 to 300 K for (c) P-TAME, (d) TAPR, and (e) P-TAPE (Inset: temperature-dependent PL spectra). (f) The PL spectra of P-TA-CPs (λ_{ex} = 420 nm).

UV-vis absorption spectra were conducted to evaluate the optical properties of these polymers. A similar broad absorption region from 380 to 550 nm was detected (Figure 2a), indicating all these polymers are visible-light responsive. Accordingly, their optical bandgaps can be calculated as 2.24 eV, 2.30 eV and 2.35 eV for P-TAME, P-TAPR and P-TAPE, respectively (Figure S10). Such narrow bandgaps may be largely attributed to the strong electron push-pull interactions between TA and Py species. Besides, determined by the Mott-Schottky profiles (Figure S11), the flat-band potentials of P-TAME, P-TAPR and P-TAPE were estimated to be of -0.95 V, -0.92 V and -0.87 V, respectively. Furthermore, the band structures of these polymers can be portrayed (Figure 2b). Note that all these polymers can trigger photocatalytic reduction and oxidation reactions in principle,

regarding their suitable conduction band (CB) and valence band (VB) levels. On one hand, no distinct difference in the CB position was observed for these polymers because of their similar chemical structures, ensuring sufficient thermodynamic driving force for photocatalytic reductions. On another hand, P-TAPE experiences the most positive VB potential, followed by P-TAPR and P-TAME, indicating P-TAPE may undergo promoted photocatalytic activity in water oxidation reaction[2b]. Thus, we can surmise that the P-TA-CPs are promising for photocatalysis.

To clarify the electron-hole pairs recombination and separation kinetics after the integration of TA units with different alkyl chains into the polymers, the temperature-dependent photoluminescence (PL) spectra of these polymers were recorded. Clearly, all polymers underwent the thermal quenching of their PL emission in the temperature range of 15-300 K (Figure 2c-e). By fitting the integrated PL intensities as a function of temperature using the Arrhenius equation: $I(T) = I_0/(1 + A\ exp(-E_b/-k_BT))$, the exciton binding energy (E_b) could be deduced as ~31, 43, and 50 meV for P-TAME, P-TAPR and P-TAPE, respectively[6a]. Since the E_b values in polymers are typically higher than 100 meV, the much lowered E_b values for P-TA-CPs can endow facilitated exciton dissociation for photocatalysis[4b]. Moreover, the PL emission intensity gradually decreased from P-TAPE to P-TAME (Figure 2f), implying P-TAME experiences the most suppressed charge recombination, which could be a positive effect on the photocatalytic activity.

Table 1. Physicochemical properties of the P-TA-CPs.

Polymer[b]	Average charges A[c] [e]	E_b[b] [meV]	HER[c] [μmol h^{-1}]	S_{BET}[d] [m^2 g^{-1}]
P-TAME	-0.53	31	100	675
P-TAPR	-0.50	43	70	412
P-TAPE	-0.48	50	20	19

[a] The average of the Bader charges of TA moieties by DFT calculations and a negative value means getting electrons. [b] Exciton binding energy (E_b) of the PL quenching process in the P-TA-CPs. [c] Reaction conditions: 10 mg polymer, TEOA/H_2O (10 mL/100 mL), 300 W Xe lamp, λ > 420 nm, 12 ºC. [d] Specific surface area was calculated from the N_2 sorption isotherms.

To gain theoretical insights, the HOMO/LUMO levels and the Bader charges in each polymer were calculated by the density functional theory (DFT) employing the fragmental structures (Figure S12). Notably, all the CPs feature spatially separated HOMO and LUMO delocalization demonstrating that the charge carrier recombination could be greatly restrained and thus beneficial to the charge separation for these CPs in theory, in good accordance with their low E_b values. Bader charge analysis can provide useful information in evaluating electronic and charge transfer behaviors. Accordingly, the average charges of acceptor fragment units (i.e., TA) were summarized (Table 1, average charges-A). Prominently, the electron-withdrawing ability of TA was strengthened along with the decrement of alkyl chain length anchored in the polymers. Consequently, the strongest D-A interactions may be generated for P-TAME among the series and thus have a great chance to reduce the Coulomb electrostatic interactions, leading to the minimized E_b. Indeed, the results are in line with the tendency of E_b values. Hence, the side-chain molecular engineering approach conceived in this study is a reliable protocol to tune the charge migration kinetics during photocatalysis.

Photoelectrochemical characterizations can provide further information about the charge migration behaviors in these CPs. The photocurrent experimental results (Figure S13) revealed that P-TAME could give rise to a much stronger photocurrent response than P-TAPR and P-TAPE, signifying less recombination and faster light-induced electron migration in P-TAME. The order for photocurrent responsiveness of these three polymers has much to do with their electron-donating and withdrawing ability in the D-A system, the stronger the D-A interactions, the better transportation of charge. Likewise, P-TAME also manifested a smaller radius than P-TAPR and P-TAPE in electrochemical impedance spectroscopy (EIS) tests upon dark or light irradiation (Figure S14), implying a low charge transfer resistance and more rapid interfacial electron transfer in P-TAME. All these results are consistent with the conclusions drawn from DFT and PL analyses, which is again highlighting the critical role of side chain-engineered novel triazole-based D-A systems in the efficient splitting of photoexcited charge carriers.

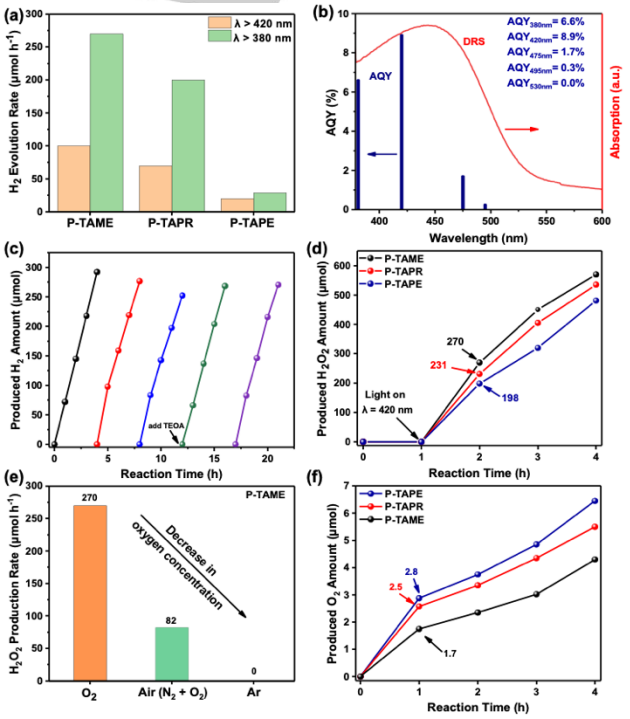

Figure 3. Photocatalytic performances of P-TA-CPs. a) H_2 evolution rates. b) The wavelength-dependent of the AQYs of P-TAME. c) Long-term H_2 evolution by P-TAME. d) Time dependence of H_2O_2 generation under visible light irradiation; Conditions: 20 mg polymer, 2 mL phenylcarbinol, 18 mL H_2O, 1 atm O_2, 298 K, 420 nm LED. e) Influence of O_2 concentration on the H_2O_2 production rate of P-TAME in the presence of phenylcarbinol. f) O_2 evolution rates under visible-light irradiation.

The particle dispersibility and favorable interactions with water are crucial for efficient heterogeneous photocatalysis. Therefore, the water contact angles (WCA) on these polymers' surfaces were first evaluated. The results revealed that the WCA orderly decreases from 159.9° for P-TAME to 42.5° for P-TAPE with the increment of the length of alkyl chains (Figure S15), demonstrating the reduced surface hydrophilicity from P-TAME to P-TAPE. Moreover, to elucidate the water accessibility of the internal pore structures of these polymers, water vapor uptake experiments were performed. All the polymers feature type III

isotherms (Figure S16), and P-TAME adsorbs ~56 wt% water at 298 K and 50.3 mbar. In contrast, P-TAPR and P-TAPE only adsorb ~17 and 10 wt% water under the same conditions. This may be caused by the water condensation within the pore of P-TAME, which is decorated with the shortest alkyl chains. In this regard, P-TAME experiences the best water wettability, both inside the pore structure and the external surface, thus increasing the number of potential sites for heterogenous photocatalysis, apt to realize a promoted photocatalytic activity.

H_2 production reaction was first carried out. Regarding the residual palladium in the polymer skeletons (Pd Content: 0.28-0.36 wt.%, Table S2) as plausible cocatalyst[5b, 18], the reactions were conducted without adding Pt cocatalyst. As expected, the P-TAME (10 mg) illustrates the best hydrogen evolution rate (HER) of ~100 μmol h^{-1} under visible light irradiation (λ > 420 nm) and ~270 μmol h^{-1} under broadband light irradiation (λ > 300 nm) (Figure 3a), and an apparent quantum yield (AQY) of 8.9% at 420 nm was achieved (Figure 3b). After screening various sacrificial agents and dosages of the polymer, the HER of P-TAME was further increased to ~110 μmol h^{-1} (15 mg polymer, TEOA as the sacrificial agent, Figure S17). These values surpass most reported Py-based CPs with different acceptors (Table S3), clarifying their promising potential as an organic photocatalyst. Besides, the wavelength-dependent AQY of H_2 generation over P-TAME was also uncovered (Figure 3b). A good match between the AQYs and UV-vis DRS was observed, suggesting that the H_2 production is primarily induced by the photoexcited electrons. Moreover, the HER activity of P-TAME (Figure 3c) remained almost the same level during the 5-circles test (20 h), verifying a stable photocatalysis of P-TAME. When P-TAME was recovered and re-characterized by PXRD (Figure S18) and FTIR (Figure S19), no apparent change observed, strongly exemplifying its robust stability upon solution and light corrosion.

Photocatalytic H_2O_2 production is a promising alternative route to the traditional anthraquinone process, which has aroused universal interest recently[19]. Very interestingly, the excellent photocatalytic activity of these polymers for H_2O_2 production was feasibly evidenced. Indeed, all these three polymers can trigger oxygen reduction (ORR) to produce H_2O_2 and the amount increased steadily with prolonged irradiation time (Figure 3d). Satisfactorily, P-TAME (20 mg) achieves an average H_2O_2 production rate (HPPR) of ~190 μmol h^{-1}, followed by P-TAPR (~178 μmol h^{-1}) and P-TAPE (~160 μmol h^{-1}) with phenylcarbinol as the sacrificial agent, respectively. Besides, the P-TAME can also be employed as photocatalyst for triggering ORR in pure water with an average HPPR of ~38 μmol h^{-1} (Figure S20a). It is noteworthy that photocatalytic H_2O_2 production by polymers has rarely been explored thus far and the performances here surpass most of the reported polymers (Table S4). Moreover, the HPPR tendency is in good accordance with their HERs, again emphasizing the validity of molecular engineering. To figure out the H_2O_2 production mechanism, we further conducted the same reaction in different atmospheres. As shown in Figure 3e and Figure S20b, the HPPR for P-TAME was highest in pure O_2, much lower in air, and completely prohibited in Ar, suggesting H_2O_2 generated through the ORR process. The strongest D-A interactions induced facilitated-charge-separation and promoted-charge-migration might be mainly accounted for the highest photocatalytic HER and HPPR associated with P-TAME.

As a control, we prepared two other polymer photocatalysts based on typical electron-deficient units, i.e., P-FSO and P-BT (Scheme S1-S2). Compared with P-FSO and P-BT, P-TAME demonstrated better photocatalytic HER (10 mg polymer) and HPPR (20 mg polymer) under visible light irradiation (Figure S21), verifying the TA moieties as promising new electron-acceptor motifs developed in this study.

Water oxidation reaction (WOR) involves four-electron transfer with O-H bond cleavage and new O-O bond formation, necessitating a huge activation energy and usually resulting in a relatively slow reaction speed and low activity[20]. Given the unique band structures of these polymers, the WOR could occur theoretically by using them as photocatalysts. To clarify this assumption, the photocatalytic WOR was subsequently proceeded by employing these polymers as the photocatalysts and $AgNO_3$ as the sacrificial agent. Indeed, all these polymers can mediate the WOR and the P-TAPE (25 mg) afforded the best activity with a total O_2 evolution rate (OER) of ~ 6.5 μmol after 4 h under visible light irradiation (λ > 420 nm, Figure 3f). This result corresponds to the most positive VB level for P-TAPE**.**

In summary, a series of novel TA-based D-A-type conjugated polymers with varied alkyl chains anchored in the skeletons have been tailor-made to address the effect of molecular engineering on the band structures, D-A interactions, as well as the charge separation and migration kinetics. All these polymers feature suitable band structures and similar CB levels, rendering them promising photocatalysts for photocatalytic reductions. Due to the presence of the strongest electron push-pull interactions, P-TAME features the minimized E_b and thus realizes a promoted charge separation. Combining with the suppressed charge recombination and facilitated charge transfer, P-TAME shows outstanding photocatalytic performances for HER and HPPR. Interestingly, these polymers can also be used as photocatalysts to trigger WOR to liberate oxygen from water. By further rational design of the TA units or other donor moieties at the molecular level, more TA-based D-A-type polymers with high photocatalytic performances could be achieved with even enthusiastic dreamed photocatalytic overall water splitting in the future.

Acknowledgments

This work was financially supported by the National Natural Science Foundation of China (21972021, U1905214 and 22111530111), the Chang Jiang Scholars Program of China (T2016147), and the 111 Project (D16008).

Keywords: triazole polymers • semiconductors • photocatalysts • H_2O_2 production • H_2 evolution

[1] a) J. M. Lee, A. I. Cooper, *Chem. Rev.* **2020**, *120*, 2171-2214; b) C. Shu, C. Han, X. Yang, C. Zhang, Y. Chen, S. Ren, F. Wang, F. Huang, J. X. Jiang, *Adv. Mater.* **2021**, *33*, e2008498.

[2] a) X. Wang, K. Maeda, A. Thomas, K. Takanabe, G. Xin, J. M. Carlsson, K. Domen, M. Antonietti, *Nat. Mater.* **2009**, *8*, 76-80; b) G. Li, Z. Xie, S. Chai, X. Chen, X. Wang, *Appl. Catal. B: Environ.* **2021**, *283*, 19637; c) Z. Xie, W. Wang, X. Ke, X. Cai, X. Chen, S. Wang, W. Lin, X. Wang, *Appl. Catal. B: Environ.* **2023**, *325*, 122312.

[3] a) E. Jin, Z. Lan, Q. Jiang, K. Geng, G. Li, X. Wang, D. Jiang, *Chem* **2019**, *5*, 1632-1647; b) L. Cusin, H. Peng, A. Ciesielski, P. Samori, *Angew. Chem. Int. Ed.* **2021**, *60*, 14236-14250; c) L. Zhai, Z. Xie, C. X. Cui, X. Yang, Q. Xu, X. Ke, M. Liu, L. Qu, X. Chen, L. Mi, *Chem. Mater.* **2022**, *34*, 5232-5240; d) 4.Z. Xie, X. Yang, P. Zhang, X. Ke, X. Yuan, L. Zhai, W. Wang, N. Qin, C. X. Cui, L. Qu, X. Chen. *Chin. J. Catal.* **2023**, *47*, 171-180.

[4] a) R. S. Sprick, B. Bonillo, R. Clowes, P. Guiglion, N. J. Brownbill, B. J. Slater, F. Blanc, M. A. Zwijnenburg, D. J. Adams, A. I. Cooper, *Angew.*

Chem. Int. Ed. **2016**, *128*, 1824-1828; b) Z. A. Lan, G. Zhang, X. Chen, Y. Zhang, K. A. I. Zhang, X. Wang, *Angew. Chem. Int. Ed.* **2019**, *58*, 10236-10240; c) Y. Bai, C. Li, L. Liu, Y. Yamaguchi, M. Bahri, H. Yang, A. Gardner, M. A. Zwijnenburg, N. D. Browning, A. J. Cowan, A. Kudo, A. I. Cooper, R. S. Sprick, *Angew. Chem. Int. Ed.* **2022**, *61*, e202201299.

[5] a) R. S. Sprick, J. X. Jiang, B. Bonillo, S. Ren, T. Ratvijitvech, P. Guiglion, M. A. Zwijnenburg, D. J. Adams, A. I. Cooper, *J. Am. Chem. Soc.* **2015**, *137*, 3265-3270; b) G. Li, Z. Xie, Q. Wang, X. Chen, Y. Zhang, X. Wang, *Chem. Eur. J.* **2021**, *27*, 939-943.

[6] a) Z. A. Lan, M. Wu, Z. Fang, X. Chi, X. Chen, Y. Zhang, X. Wang, *Angew. Chem. Int. Ed.* **2021**, *60*, 16355-16359; b) Y. Liu, Z. Liao, X. Ma, Z. Xiang, *ACS Appl. Mater. Inter.* **2018**, *10*, 30698-30705.

[7] a) X. Wang, L. Chen, S. Y. Chong, M. A. Little, Y. Wu, W. H. Zhu, R. Clowes, Y. Yan, M. A. Zwijnenburg, R. S. Sprick, A. I. Cooper, *Nat. Chem.* **2018**, *10*, 1180-1189; b) Z. A. Lan, W. Ren, X. Chen, Y. Zhang, X. Wang, *Appl. Catal. B: Environ.* **2019**, *245*, 596-603; c) D. J. Woods, S. A. J. Hillman, D. Pearce, L. Wilbraham, L. Q. Flagg, W. Duffy, I. McCulloch, J. R. Durrant, A. A. Y. Guilbert, M. A. Zwijnenburg, R. S. Sprick, J. Nelson, A. I. Cooper, *Energy Environ. Sci.* **2020**, *13*, 1843-1855; d) W. Chen, L. Wang, D. Mo, F. He, Z. Wen, X. Wu, H. Xu, L. Chen, *Angew. Chem. Int. Ed.* **2020**, *59*, 16902-16909.

[8] a) M. Cocchi, J. Kalinowski, V. Fattori, J. A. G. Williams, L. Murphy, *Appl. Phys. Lett.* **2009**, *94*, 073309; b) A. S. Kostyuchenko, L. Y. V, A. Kurowska, W. Domagala, A. Pron, A. S. Fisyuk, *Beilstein J. Org. Chem.* **2014**, *10*, 1596-1602; c) J. Zhuang, W. Su, W. Li, Y. Zhou, Q. Shen, M. Zhou, *Org. Electron.* **2012**, *13*, 2210-2219.

[9] a) B. Campagne, G. David, B. Améduri, D. J. Jones, J. Rozière, I. Roche, *Macromolecules* **2013**, *46*, 3046-3057; b) W. Li, X. Liang, H. Niu, Z. Tu, J. Feng, M. Pan, H. Zhang, *J Colloid. Interf. Sci.* **2014**, *432*, 26-30.

[10] a) D. Caceres, C. Cebrian, A. M. Rodriguez, J. R. Carrillo, A. Diaz-Ortiz, P. Prieto, F. Aparicio, F. Garcia, L. Sanchez, *Chem. Commun.* **2013**, *49*, 621-623; b) M. J. Pastor, I. Torres, C. Cebrian, J. R. Carrillo, A. Diaz-Ortiz, E. Matesanz, J. Buendia, F. Garcia, J. Barbera, P. Prieto, L. Sanchez, *Chem. Eur. J* **2015***, 21,* 1795-1802

[11] E. Lim, *Int. J. Photoenergy* **2013**, *2013*, 1-7.

[12] a) T. Yasuda, K. Namekawa, T. Iijima, T. Yamamoto, *Polymer* **2007**, *48*, 4375-4384; b) D. Dontsova, S. Pronkin, M. Wehle, Z. Chen, C. Fettkenhauer, G. Clavel, M. Antonietti, *Chem. Mater.* **2015**, *27*, 5170-5179.

[13] V. S. Vyas, F. Haase, L. Stegbauer, G. Savasci, F. Podjaski, C. Ochsenfeld, B. V. Lotsch, *Nat. Commun.* **2015**, *6*, 8508.

[14] a) G. P. Mane, S. N. Talapaneni, K. S. Lakhi, H. Ilbeygi, U. Ravon, K. Al-Bahily, T. Mori, D. H. Park, A. Vinu, *Angew. Chem. Int. Ed.* **2017**, *56*, 8481-8485; b) H. Wang, M. Li, Q. Lu, Y. Cen, Y. Zhang, S. Yao, *ACS Sustain. Chem. Eng.* **2018**, *7*, 625-631.

[15] a) C. Han, P. Dong, H. Tang, P. Zheng, C. Zhang, F. Wang, F. Huang, J. X. Jiang, *Chem. Sci.* **2020**, *12*, 1796-1802; b) S. Chai, X. Chen, X. Zhang, Y. Fang, R. S. Sprick, X. Chen, *Environ. Sci. Nano* **2022**, *9*, 2464-2469.

[16] a) I. A. Arkhipushkin, M. O. Agafonkina, L. P. Kazansky, Y. I. Kuznetsov, K. S. Shikhaliev, *Electrochim. Acta* **2019**, *308*, 392-399; b) C. Cheng, B. He, J. Fan, B. Cheng, S. Cao, J. Yu, *Adv. Mater.* **2021**, *33*, e2100317; c) D. B. Wang, B. H. Chen, B. Zhang, Y. X. Ma, *Polyhedron* **1997**, *16*, 2625-2629.

[17] G. Liu, Y. Huang, X. Qu, J. Xiao, X. Yang, Z. Xu, *Colloid. Surface. A* **2016**, *503*, 34-42.

[18] a) L. Li, Z. Cai, Q. Wu, W. Y. Lo, N. Zhang, L. X. Chen, L. Yu, *J. Am. Chem. Soc.* **2016**, *138*, 7681-7686; b) J. Kosco, M. Sachs, R. Godin, M. Kirkus, L. Francas, M. Bidwell, M. Qureshi, D. Anjum, J. R. Durrant, I. McCulloch, *Adv. Energy Mater.* **2018**, *8*, 1802181; c) M. Sachs, H. Cha, J. Kosco, C. M. Aitchison, L. Francaś, S. Corby, C. L. Chiang, A. A. Wilson, R. Godin, A. Fahey-Williams, A. I. Cooper, R. S. Sprick, I. McCulloch, J. R. Durrant, *J. Am. Chem. Soc.* **2020**, *142*, 14574-14587.

[19] Q. Wu, Y. Liu, J. Cao, Y. Sun, F. Liao, Y. Liu, H. Huang, M. Shao, Z. Kang, *J. Mater. Chem. A* **2020**, *8*, 11773-11780.

[20] a) Z. A. Lan, Y. Fang, Y. Zhang, X. Wang, *Angew. Chem. Int. Ed.* **2018**, *57*, 470-474; b) C. Zhao, Z. Chen, R. Shi, X. Yang, T. Zhang, *Adv. Mater,* **2020**, *32*, e1907296.

Entry for the Table of Contents

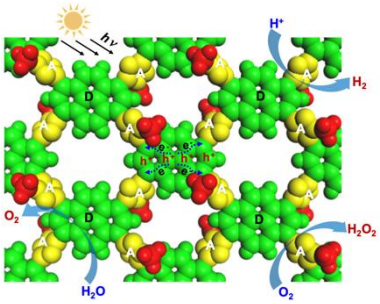

Donor−acceptor polymer photocatalysts bearing alkyl chains were synthesized to explore the effect of side-chain engineering on charge separation and migration kinetics. High activity was reached in photocatalytic reduction reactions with promoted exciton dissociation, suppressed charge recombination, facilitated charge transfer, and favorable hydrophilicity. Key: donor (D), acceptor (A), pyrene (green), triazole (yellow), methyl (red).